Applied Catalysis B: Environmental 129 (2013) 549–555

Contents lists available at SciVerse ScienceDirect

Applied Catalysis B: Environmental

journal homepage: www.elsevier.com/locate/apcatb

A high-efficiency microwave approach to synthesis of Bi-modified Pt nanoparticle catalysts for ethanol electro-oxidation in alkaline medium

Yiyin Huang, Jindi Cai, Yonglang Guo*

College of Chemistry and Chemical Engineering, Fuzhou University, Fuzhou 350108, PR China

ARTICLE INFO

Article history:
Received 18 June 2012
Received in revised form
11 September 2012
Accepted 18 September 2012
Available online 8 October 2012

Keywords:
Alkaline fuel cell
Bi modification
Ethanol oxidation
Microwave synthesis
Pt catalyst

ABSTRACT

The Bi-modified Pt nanoparticle catalysts using multi-walled carbon nanotubes as supports are prepared through microwave treatment and long-term standing approaches. Bi can easily modify Pt catalyst because of the strong affinity between Bi and Pt. However, only limited amount of Bi and uneven Bi-modified Pt catalyst are obtained through the long-term standing approach. The microwave approach can complete the synthesis rapidly and get uniform Bi–Pt/CNT catalysts. X-ray photoelectron spectroscopy shows that Bi (III) and Pt (0) species are the main form in the Bi–Pt/CNT catalyst. Cyclic voltammetry indicates that the modification of Bi on Pt/CNTs leads to an enhanced activity up to 260% compared to Pt/CNTs for ethanol electro-oxidation. The current of Bi–Pt/CNTs (0.1:1) is 44.8 times higher than that of Pt/CNTs at −0.3 V for 1800 s. Linear current sweep results reveal that the electro-oxidation of residual intermediate species can be effectively promoted because the adsorption of OH_{ad} species is enhanced by the addition of Bi to Pt/CNTs, which is characterized by the higher open circuit potential.

1. Introduction

Direct ethanol fuel cell (DEFC) has attracted much attention in recent years due to its merits such as high energy density (8 kW h kg^{-1}), low pollutant emitting feature and easy fuel delivery and storage. Besides, ethanol is a renewable resource as it can be produced in large quantities from agricultural products and biomass, which will not change the natural balance of carbon dioxide in the atmosphere in contrast to the use of fossil fuels [1–5]. The ethanol oxidation reaction (EOR) undergoes successive dehydrogenation steps and removal of complicated adsorbed intermediates and byproducts. The complete oxidation of ethanol to CO_2 requires the cleavage of C—C bond. The C—C bond is between two atoms with little electron affinity or ionization energy, making it difficult to be broken at low temperatures [6–8]. Enhancement on both dehydrogenation steps and oxidation of poisonous species can increase the electrochemical activity of the catalyst for EOR. Therefore, high kinetics and tolerable deactivation are quite important for the design and synthesis of new anodic catalysts for ethanol oxidation.

Alkaline fuel cell (AFC) exhibits several intrinsic advantages as compared with the acidic counterpart such as wider choices of fuel feed. It has been proven that if direct alcohol fuel cell (DAFC) operates in alkaline electrolyte rather than in acidic electrolyte the reaction kinetics of both the anodic oxidation of alcohol and the cathodic reduction of oxygen will be significantly improved [9–11]. And the development of anion exchange membrane (AEM) makes the application of AFC more practicable. However, it still needs a highly effective catalyst that can promote oxidation of organic fuels at a favourable rate for the commercialization of AFC.

The catalytic activity together with selectivity towards alcohol oxidation and the tolerance towards adsorbed poisoning species can be markedly changed by the modifications on catalyst surfaces with other species, for they can modify the electronic and stereochemical properties of the substrate [12–15]. For example, heteropolyacids of tungsten and molybdenum form electroactive adsorbates on Pt surfaces and these composites exhibit fast electron transfer capabilities in the electro-reduction [16–20]. Keggin-type $H_3PW_{12}O_{40}$ and $H_3PMo_{12}O_{40}$ polyanions are also likely to facilitate the decomposition of methanol [18–20]. Modifications on Pt surfaces with p-block or transition elements such as Ru, Pb, Sn, Sb and Bi [21–24], have been proven to be effective in promoting the catalytic properties of Pt. Among these elements, Bi is known to have very significant catalytic improvement in alkaline medium [25–27]. Du and Wang reported the enhanced electro-oxidation of methanol on Pt nanoparticles modified by underpotential deposited Bi [28]. López-Cudero et al. also obtained the enhanced electro-oxidation activity of formic acid and CO on Bi modified polyoriented and preferential (1 1 1) Pt nanoparticles [29]. Simões et al. studied the glycerol electro-oxidation on Pt and Pd nanoparticle surfaces modified by Bi via a colloidal route. The greatly enhanced catalytic activities were observed [30].

* Corresponding author. Tel.: +86 591 8807 3608; fax: +86 591 8807 3608.
E-mail address: yguo@fzu.edu.cn (Y. Guo).

0926-3373/$ – see front matter © 2012 Elsevier B.V. All rights reserved.
http://dx.doi.org/10.1016/j.apcatb.2012.09.049

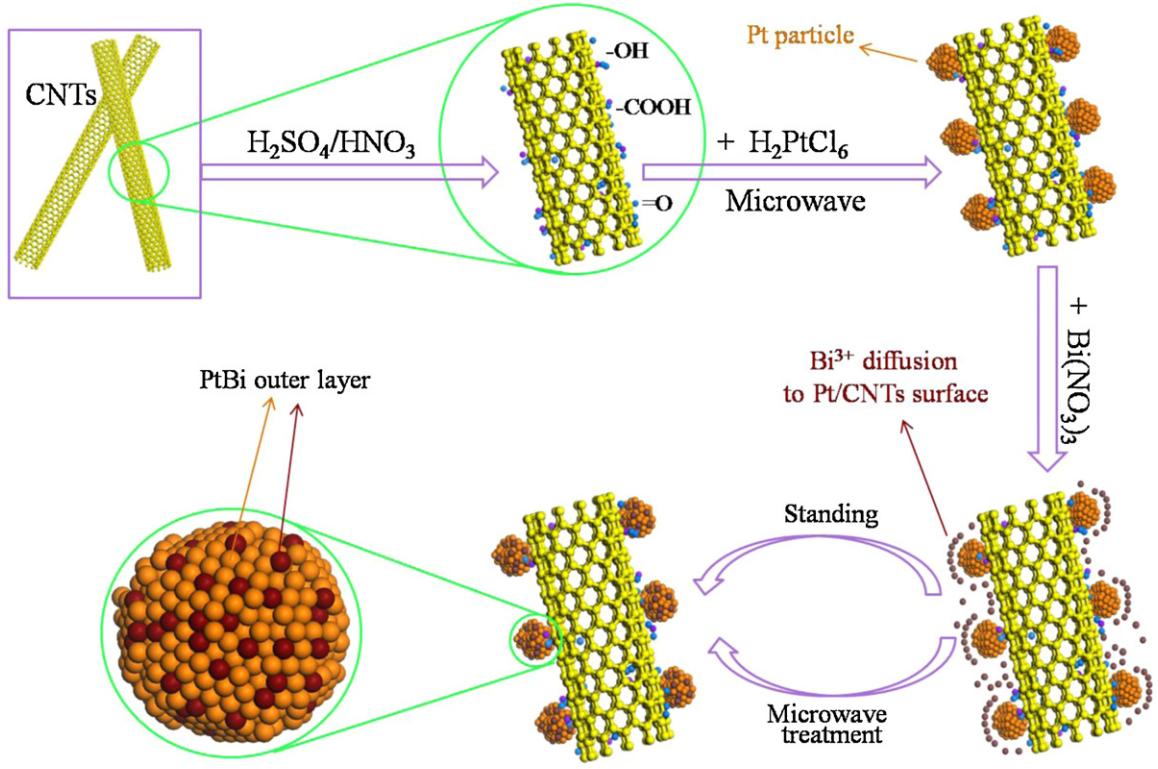

Fig. 1. Schematic illustration of the synthesis procedure of Bi–Pt/CNT catalysts.

In contrast with the conventional preparation, microwave-assisted polyol method is faster and conducive to generating colloids and clusters on the nanoscale with greater uniformity [31–33]. At present, there are very few reports about Pt nanoparticle surface modification achieved through microwave approach [34]. This study aims at employing rapid microwave-assisted polyol technique to synthesize Bi-modified Pt nanoparticles. The performances of Bi–Pt/carbon nanotube (CNT) and Pt/CNT catalysts were contrastively tested for ethanol electro-oxidation in alkaline medium. The reduction selectivity in the microwave action and the promoting mechanism of Bi were discussed.

2. Experimental

2.1. Synthesis of catalysts

Multi-walled carbon nanotubes (CNTs), purchased from Shenzhen Nanotechnologies Co. Ltd. (China), were pretreated with the mixed acids of concentrated HNO_3 and H_2SO_4 in 1:3 ratio at 120 °C for 2 h. The mixture was diluted, filtered, washed with double-distilled water and dried overnight. Bi–Pt/CNT catalysts were prepared in two methods (Fig. 1): in the first Bi–Pt/CNT preparation, 14.7 mg of CNTs and 1 ml of H_2PtCl_6 (18.9 mM) were mixed in 50 ml of ethylene glycol (EG) under ultrasonic stirring for 30 min. The mixture was then treated in the flask with a reflux set for 90 s under a microwave power of 800 W. Afterwards, 0.1 ml of $Bi(NO_3)_3$ (18.9 mM) and 1 ml of KOH (0.4 M) were added into the mixture with continuous stirring and then let the suspension stand for 1, 5 or 15 h at room temperature, respectively. The resultant suspension was filtered, and the residue was washed with double-distilled water and dried overnight at 80 °C in a vacuum oven. These prepared catalysts were defined as Bi–Pt/CNTs (1 h), Bi–Pt/CNTs (5 h) and Bi–Pt/CNTs (15 h), respectively. In the second Bi–Pt/CNT preparation, the whole process was the same except that the mixture was treated in the flask with a reflux set for 5 min under the same microwave power after adding $Bi(NO_3)_3$ instead of standing. These prepared catalysts were defined as Bi–Pt/CNTs (x:1), where x was the initial atom ratio of Bi to Pt and was equal to 0.5, 0.25, 0.1 and 0.05 based on different amounts of $Bi(NO_3)_3$ in the reactor, respectively. In order to analyse the Bi deposition on CNTs in the microwave action, Bi/CNT composites were also prepared using two methods for comparison: 15.8 mg of CNTs was mixed with 1 ml of $Bi(NO_3)_3$ (18.9 mM) and 1 ml of KOH (0.4 M) in 50 ml of EG under ultrasonic stirring for 30 min. This mixture was treated for 5 min under a microwave (MW) power of 800 W or reduced by an adequate sodium borohydride (SB) solution, respectively, and was defined as Bi/CNTs (MW) and Bi/CNTs (SB).

2.2. Physical and electrochemical characterization

The Pt loadings on Bi–Pt/CNT catalysts were determined by atomic adsorption spectroscopy (AAS, Spectr AA-220). The atomic ratios of Bi to Pt in catalysts were examined by energy-dispersive X-ray (EDX) analysis using a scanning electron microscope (SEM, Philips-FEI XL30 ESEM-TMP) equipped with a microanalyser, whose resolution power is 129 eV. The chemical valences of elements in Bi–Pt/CNTs (0.1:1) were analysed by X-ray photoelectron spectroscopy (XPS, VG ESCALAB 250) with the Al K_α X-ray source of 1486.6 eV. The chamber pressure was kept below 3×10^{-10} mbar and specific correction was conducted by using a C 1s binding energy of 284.6 eV. Structure characterization was carried out by X-ray diffraction (XRD, Philip X' Pert Pro MPP) using a Cu K_α radiation (λ = 1.5418 Å) at the scan rate of 2° min^{-1} with a step of 0.02°.

Electrochemical measurements were performed in a three-electrode cell connected to CHI 660C electrochemical working station (CH Instrument Inc.). A glassy carbon electrode (0.1256 cm^2) coated with catalyst was used as the working electrode. A Pt foil and a mercuric oxide electrode (Hg/HgO/1 M KOH, 0.098 V vs. SHE [35]) were used as the counter and reference electrodes, respectively. For working electrode preparation, specific amount of the

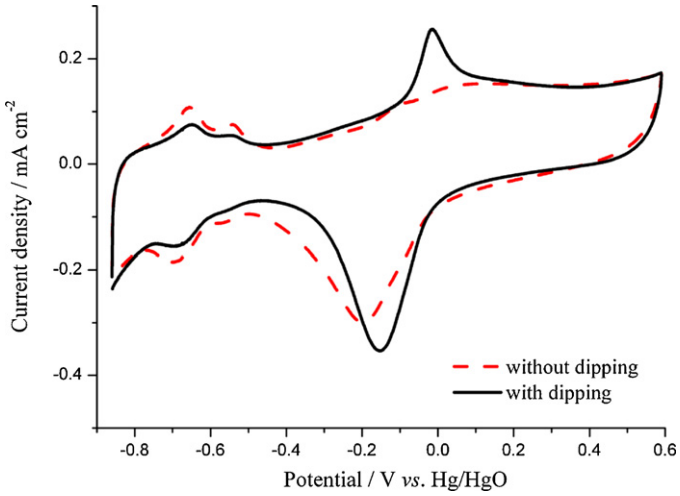

Fig. 2. Cyclic voltammograms in 1 M KOH solution of Pt electrode (0.0314 cm^2) with and without dipping in 18.9 mM $Bi(NO_3)_3$ solution for 1 h. Scan rate: 50 mV s^{-1}.

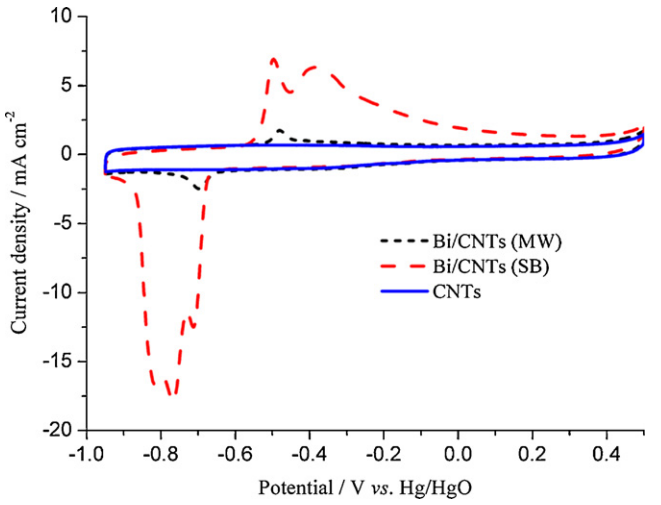

Fig. 3. Cyclic voltammograms of Bi/CNTs prepared by microwave treatment (MW) and sodium borohydride reduction (SB) and CNT electrode in 1 M KOH solution. Scan rate: 50 mV s^{-1}.

Pt-containing catalysts and 5 mg of Bi/CNT composite or CNTs were dispersed in a solution of 985 μl of isopropyl alcohol and 15 μl of 15 wt% Nafion (DuPont, USA) under ultrasonic stirring for 30 min. An 8 μl of the slurry was spread on the glassy carbon electrode surface which was first polished, rinsed and dried at 80 °C for 30 min. The total Pt loadings on working electrode surface were fixed at 8 μg. The cyclic voltammograms (CVs) were recorded in 1 M KOH or 1 M KOH + 1 M C_2H_5OH solution at the scan rate of 50 mV s^{-1} when a stable response was obtained. The electrolyte was deaerated with high purity N_2 prior to measurements. All electrochemical measurements were conducted in a thermostatic water bath at 30 °C.

3. Results and discussion

The outline of Bi–Pt/CNT catalyst fabrication is shown in Fig. 1. In the first step, a harsh treatment with concentrated H_2SO_4/HNO_3 was carried out on pristine MWCNTs to make them isolated from each other and to simultaneously produce some oxygen-containing groups on their surfaces, such as carboxyl, carbonyl and hydroxyl [36]. It has been proven that these oxygen-containing groups are crucial to the synthesis of catalysts with good uniformity and dispersion [37]. In the second step, H_2PtCl_6 was reduced under the microwave action to form Pt nanoparticles adsorbed on the surfaces of CNTs [38]. The third step was the diffusion of Bi^{3+} ions from solution to the surface of Pt/CNTs. Subsequently, the adsorption of Bi^{3+} can be achieved by two approaches. One is a long-time standing, whose availability can be proven by the spontaneously irreversible adsorption of Bi^{3+} on Pt electrode surface and then its reduction during cycling. In Fig. 2, the broken line depicts the stable cyclic voltammogram on Pt electrode in N_2-purged electrolyte. The hydrogen desorption/adsorption peaks range from −0.8 to −0.55 V. After the Pt electrode was dipped in $Bi(NO_3)_3$ solution for an hour and then washed with double-distilled water, the characteristic oxidation peak of Bi at 0 V (solid line in Fig. 2) suggests that Bi was adsorbed strongly on Pt electrode surface [30], which is further proven by the inhibited hydrogen desorption/adsorption peaks. The other is a microwave treatment. Bi is supposed to be precipitated on Pt particle surfaces by the rapid reduction of EG in the microwave action [36,39,40]. However, Bi may also be precipitated directly on the surfaces of CNTs in the microwave action, which does not fit with the original expectation. Therefore, it is necessary to estimate the Bi deposition amount on the surfaces of CNTs. The cyclic voltammograms of Bi/CNTs (MW) and Bi/CNTs (SB) prepared via different approaches are shown in Fig. 3. Some strong oxidation–reduction peaks are observed in the potential range from −0.6 to −0.2 V and from −0.6 to −0.9 V in the positive and negative-going sweeps, respectively. These peak potentials are more negative relative to the Bi peak potential in Fig. 2, which can be attributed to the difference between carbon and Pt surfaces for Bi precipitation [30,41]. Bi/CNTs (MW) prepared through the microwave approach shows extremely small redox peaks when compared to Bi/CNTs (SB) obtained from sodium borohydride reduction. Coulombic charge was obtained by the integration range from −0.6 to 0.1 V and from −0.6 to −0.95 V in Fig. 3 in the positive and negative-going sweeps, respectively, as shown in Table 1. The background correction was done via deducting the charge on CNT electrode in the corresponding potential ranges. The charge with background correction of Bi/CNTs (MW) and Bi/CNTs (SB) are 0.34 and 6.47 mC in positive-going sweeps and they are 0.23 and 6.61 mC in negative-going sweeps, respectively. Apparently, the charge of Bi/CNTs (MW) is much lower than that of Bi/CNTs (SB), revealing that Bi was not effectively precipitated on the surfaces of CNTs in the microwave action.

The Pt loadings on Bi–Pt/CNT catalysts determined by AAS analysis were 18.9 wt%, 19.6 wt%, 19.8 wt%, 20.6 wt% and 19.7 wt% for Bi–Pt/CNTs (0.5:1), Bi–Pt/CNTs (0.25:1), Bi–Pt/CNTs (0.1:1), Bi–Pt/CNTs (0.05:1) and Bi–Pt/CNTs (15 h), respectively. The EDX analysis was conducted to further verify the presence of Bi in Bi–Pt/CNT catalysts and is shown in Fig. 4. It is obvious that the BiM peak at around 2.5 keV increases with the ratio of Bi to Pt in the catalysts. The atomic ratios of Bi:Pt in Bi–Pt/CNT catalysts synthesized by the microwave and standing methods are 0.49:1, 0.27:1, 0.095:1, 0.059:1 and 0.046:1 for Bi–Pt/CNTs (0.5:1), Bi–Pt/CNTs (0.25:1), Bi–Pt/CNTs (0.1:1), Bi–Pt/CNTs (0.05:1) and Bi–Pt/CNTs (15 h), respectively. In the synthesis of the microwave treatment and long-term standing, the adding Bi amount in the reactor is the same for Bi–Pt/CNTs (0.1:1) and Bi–Pt/CNTs (15 h). However, the practical Bi content in Bi–Pt/CNT (15 h) in Fig. 4 is less than that

Table 1
Coulombic charge of oxidation–reduction peaks on CNTs, Bi/CNTs (SB) and Bi/CNTs (MW) in 1 M KOH.

	Anodic peak charge/mC	Cathodic peak charge/mC
CNTs background	1.19	0.98
Bi/CNTs (SB)	6.47	6.61
Bi/CNTs (MW)	0.34	0.23
Ratio of (MW)/(SB)	5.25%	3.48%

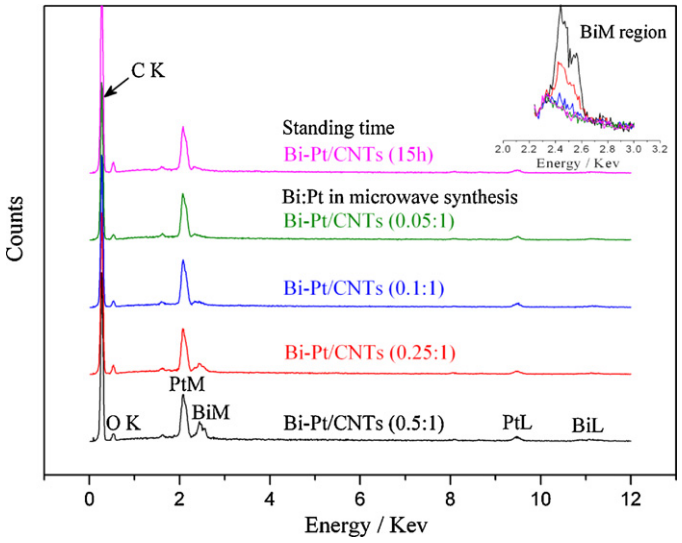

Fig. 4. EDX patterns of Bi–Pt/CNT catalysts prepared via standing and microwave synthesis approaches. The inset is the amplification of BiM peaks.

in Bi–Pt/CNTs (0.1:1). Obviously, the diffusion of Bi^{3+} ions to the surface of Pt/CNT particles is slow in EG solution which has a high viscosity. In the microwave treatment, however, the temperature of the reaction system can elevate to boiling point of EG (197.8 °C) rapidly within 1 min, which reduces the viscosity of EG and accelerates the diffusion of Bi^{3+} ions greatly. Therefore, the Bi^{3+} ions can easily reach the surface of Pt/CNT particles and deposit as hydroxide or oxide in alkaline medium in the microwave treatment for 5 min.

The XRD patterns for the prepared catalysts are presented in Fig. 5. For all catalysts, the diffraction peak at 24.9° is corresponding to the (0 0 2) plane of graphitized CNTs and the three main peaks at 39.7°, 46.3° and 68.4° are assigned to Pt (1 1 1), (2 0 0) and (2 2 0) planes of the Pt *fcc* crystal (JCPDS-ICDD, Card No. 04-802), respectively. No obvious diffraction peaks related to Bi or Bi oxides are found on Bi–Pt/CNTs (15 h), Bi–Pt/CNTs (0.05:1) and Bi–Pt/CNTs (0.1:1) because the Bi content is low and these species may exist in amorphous phases. There are some small peaks at ca. 32° on Bi–Pt/CNTs (0.25:1) and Bi–Pt/CNTs (0.5:1). These peaks are caused by the diffraction of Bi_2O_3 and little Bi_4O_7 probably located

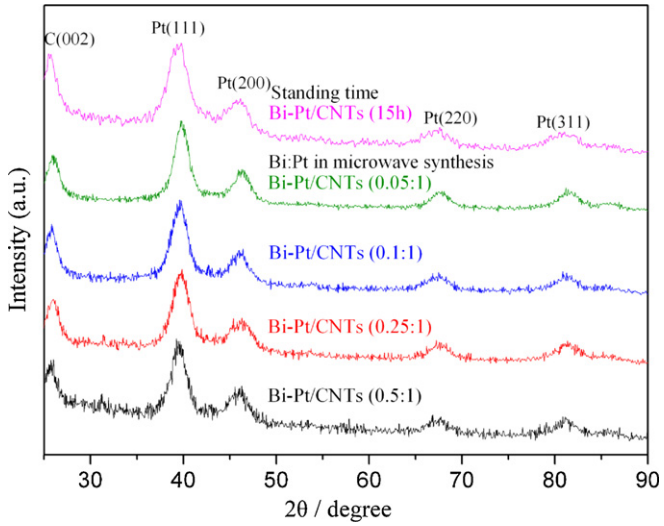

Fig. 5. XRD patterns of Bi–Pt/CNT catalysts prepared via standing and microwave synthesis approaches.

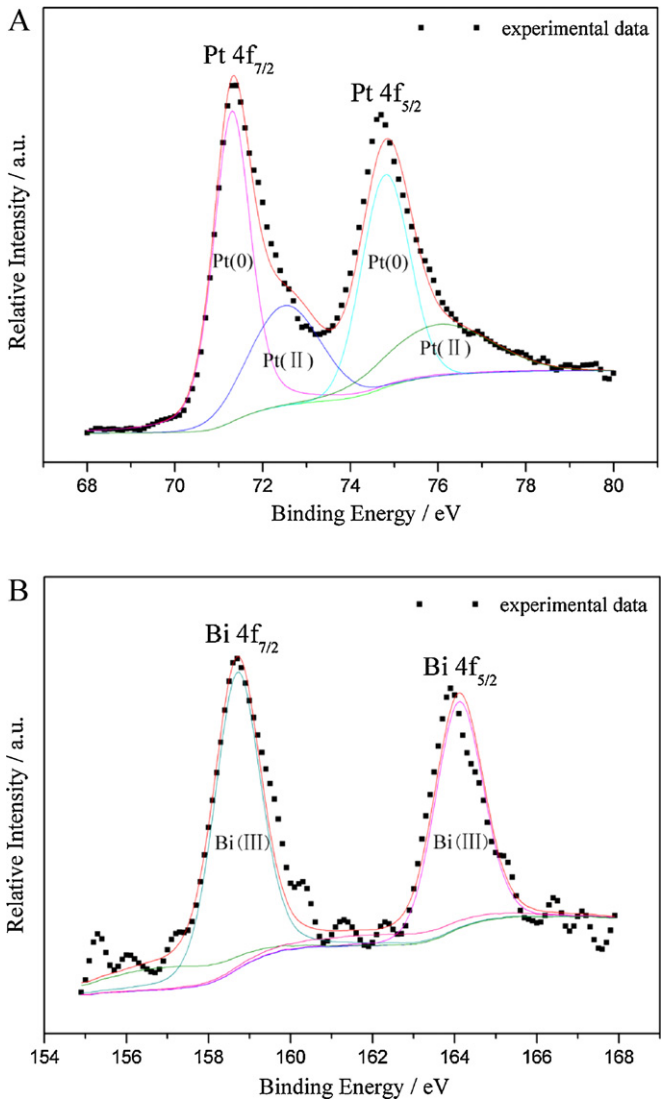

Fig. 6. XPS spectra of Bi–Pt/CNTs (0.1:1) prepared via the microwave synthesis approach: (A) Pt 4f and (B) Bi 4f regions.

on CNT surfaces (JCPDS-ICDD, Card Nos. 65-3319 and 47-1058). XPS spectra were used to determine the valence states of Pt and Bi in Bi–Pt/CNT (0.1:1) catalyst, as shown in Fig. 6. Pt 4f signal consists of two pairs of doublets and the binding energies (BEs) of Pt $4f_{5/2}$ (74.6 and 76.2 eV) are about 3.5 eV higher than those of Pt $4f_{7/2}$ (71.1 and 72.7 eV) in each doublet (Fig. 6A). The intense doublet belongs to Pt (0) and the weak one is assigned to Pt (II) species, such as PtO and $Pt(OH)_2$. For Bi 4f region in Fig. 6B, the peaks of Bi $4f_{7/2}$ and $4f_{5/2}$ at 158.8 and 164.1 eV are attributed to Bi (III). Very small fitting peaks are assigned to Bi (0), suggesting that most of Bi was deposited as hydroxide or oxide in alkaline medium on the Pt/CNT surface. Therefore, Bi (III) oxide is the main species in Bi–Pt/CNT catalysts.

Stable cyclic voltammograms in 1 M KOH solution of different Bi–Pt/CNT catalysts synthesized by two different synthesis approaches are shown in Fig. 7, and the resultant currents are normalized with respect to the electrode apparent area (0.1256 cm^2). The hydrogen desorption/adsorption peaks are inversely proportional to the oxidation peaks of Bi at 0 V. Although the same Bi^{3+} amount is added to the reactors for synthesizing different catalysts in Fig. 7, the order of Bi oxidation peak area is Bi–Pt/CNTs (0.1:1) > Bi–Pt/CNTs (5 h) = Bi–Pt/CNTs (15 h) > Bi–Pt/CNTs (1 h). It means that the adsorption of Bi^{3+} ions on the Pt/CNTs increases

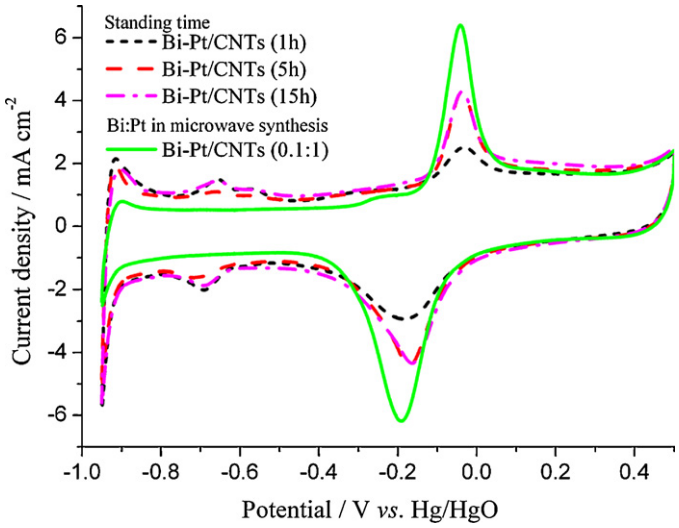

Fig. 7. Cyclic voltammograms of different Bi–Pt/CNT catalysts in 1 M KOH solution. Scan rate: 50 mV s^{-1}.

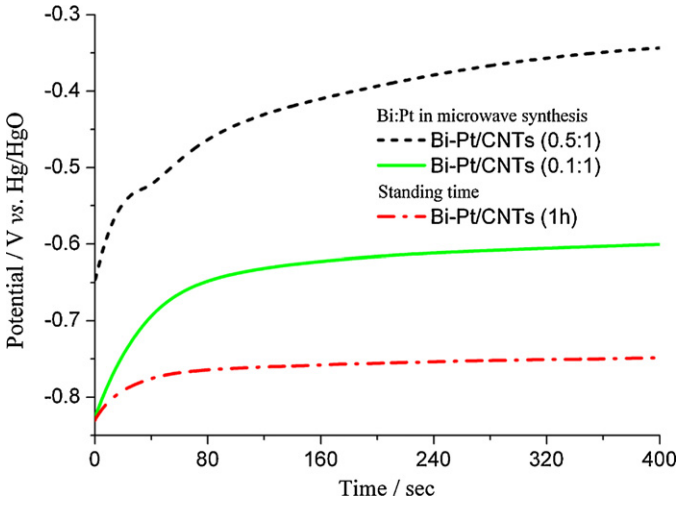

Fig. 9. The change of the open circuit potential on different Bi–Pt/CNT catalysts after 10 cycles in 1 M KOH solution.

with the standing time and tends to a saturation after 5 h. The Bi^{3+} ions only adsorb and aggregate on the outside of Pt/CNT particles through slow diffusion, which can inhibit Bi^{3+} ions to further access the catalyst surface because of the repulsion of high valence ions. Under the microwave action, however, the adsorbed Bi^{3+} ions outside of Pt/CNT particles can be easily dispersed into the interior of the catalyst aggregation and interacts with Pt with strong affinity to synthesize Bi–Pt/CNT catalysts.

The cyclic voltammograms in 1 M KOH solution of different Bi–Pt/CNT catalysts prepared via the microwave approach with different initial atomic ratios of Bi to Pt are shown in Fig. 8. With the increase of Bi amount in Bi–Pt/CNTs, the peak of Bi oxidation increases obviously, while the hydrogen desorption/adsorption peaks decreases. It suggests Bi aggregates on Pt particle surfaces, which is in agreement with the results in Fig. 7. The Bi–Pt/CNTs (0.5:1) catalyst has very small peaks related to hydrogen desorption/adsorption in the potential from −0.9 to −0.6 V, indicating that the Pt active sites are very limited. It is demonstrated that Bi is concentrated on the Pt surfaces through sodium borohydride reduction approach [22]. The strong affinity between Bi and Pt enables the

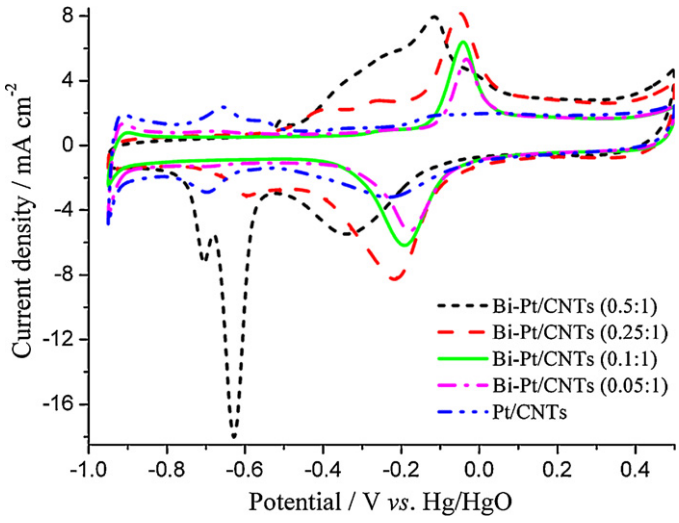

Fig. 8. Cyclic voltammograms of Bi–Pt/CNT catalysts with different atomic ratios of Bi to Pt in microwave synthesis and Pt/CNT catalyst in 1 M KOH solution. Scan rate: 50 mV s^{-1}.

modification of the Bi^{3+} adsorption on Pt catalysts [28,29], which could also be the main reason for the Bi aggregation on Pt particle surfaces in the microwave action. Bi is difficult to be directly precipitated on CNT surfaces in the microwave action without the presence of Pt, as illustrated in Fig. 3. However, it can still be deposited as its oxides on CNT surfaces when its amount is large and the Pt particle surfaces are fully covered (see Bi–Pt/CNTs (0.5:1)), which is in agreement with XRD analysis.

It is well known that the stable open circuit potential reflects the relative balance of superficial redox reactions. The work by Peng et al. indicated that the oxygen-containing species that naturally formed on Pt surfaces can lead to a more positive open circuit potential [24]. The potential–time curves recorded after 10 CV cycles on Bi–Pt/CNT catalysts with different Bi contents in 1 M KOH solution are presented in Fig. 9. It is found that the open circuit potential moves positively with the Bi content increase, which is caused by the mixed potential in the presence of Bi hydroxide or oxide species on Pt surface. It is widely accepted that these oxygenated species is critical to the electro-catalytic oxidation of ethanol because they can enhance the tolerance towards residual intermediate species poisoning via a bifunctional mechanism [42,43].

Ethanol oxidation on Bi–Pt/CNT catalysts deriving from two synthesis approaches was performed by using CV in 1 M KOH + 1 M C_2H_5OH at a scan rate of 50 mV s^{-1}, as shown in Fig. 10. It is clear that Bi/CNTs (SB) has no activity for ethanol oxidation. However, the addition of Bi in Pt/CNTs has a promoting effect on ethanol electrooxidation. The potentials of ethanol oxidation start at around −0.7 V for all electrocatalysts and the peak currents of the ethanol oxidation increase distinctly with the increase of Bi content which has been characterized by EDX patterns and the Bi oxidation peaks at about 0 V in Fig. 7. The CVs of Bi–Pt/CNT catalysts synthesized by the microwave treatment and with different atomic ratios of Bi to Pt in 1 M KOH + 1 M C_2H_5OH solution are shown in Fig. 11. With increasing ratio of Bi to Pt in the catalyst, the catalytic activity towards ethanol oxidation displays a trend of first increase and then decrease. Pt active sites may not be fully modified and promoted by Bi on the Bi–Pt/CNT catalysts with low Bi contents, while very high Bi contents may lead to the excess coverage of Pt active sites where EOR happens (see Fig. 8). Therefore, the EOR on Bi–Pt/CNT (0.1:1) catalyst has the highest peak and exhibits over 2.6 times higher specific activity (259.3 mA cm^{-2}) than the value of Pt/CNT catalyst (98.7 mA cm^{-2}).

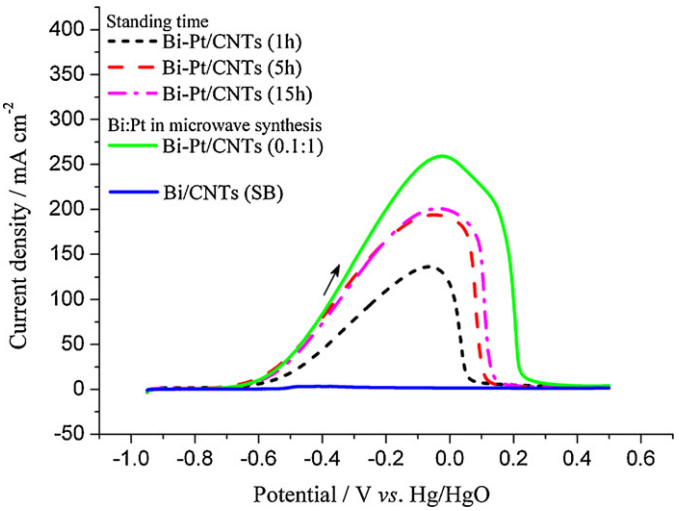

Fig. 10. Positive-going potential sweep curves of different Bi–Pt/CNT catalysts and Bi/CNTs (SB) in 1 M KOH + 1 M C_2H_5OH solution. Scan rate: 50 mV s^{-1}.

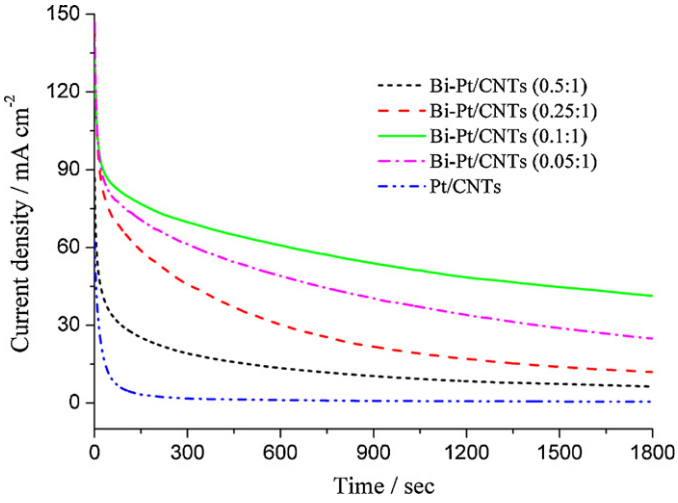

Fig. 12. Current–time curves of Bi–Pt/CNTs with different atomic ratios of Bi to Pt in microwave synthesis and Pt/CNTs at −0.3 V in 1 M KOH + 1 M C_2H_5OH solution.

Chronoamperometry was used to evaluate the promoting effect of Bi in the long-term EOR processes. The current–time curves of Bi–Pt/CNT catalysts with different atomic ratios were recorded in 1 M KOH + 1 M C_2H_5OH solution with a polarization potential of −0.3 V (vs. Hg/HgO) for 1800 s, as shown in Fig. 12. For all catalysts, there is an initial stage in which the current densities fall quickly. It should be attributed to the accumulations of poisonous carbonaceous intermediates on the catalyst surface. After that, the currents drop slowly and the electrode reactions reach the relative steady state in which the adsorptions of oxygenated species and CO-like species keep a relative balance [44–46]. The addition of Bi enhances the catalytic durability of the Pt/CNT catalyst. The final current densities increase in the following order: Pt/CNTs < Bi–Pt/CNTs (0.5:1) < Bi–Pt/CNTs (0.25:1) < Bi–Pt/CNTs (0.05:1) < Bi–Pt/CNTs (0.1:1). Unlike in acid medium, the OH_{ad} species are produced in the discharge of the OH^- in alkaline medium, not through water decomposition like on Sn or Ru sites [47–49]. In reality, it was reported that the function of Bi is to enhance the adsorption of OH_{ad} species and then to facilitate the oxidative removal of poisoning species [27,49]. From this point of view, the catalyst may have better tolerance towards CO poisoning when it contains more Bi. However, excessive Bi coverage on Pt surfaces will reduce the active sites of Pt as shown in Fig. 8. Thus, the activity and stability are better when the ratio of Bi to Pt is 0.1:1 in Bi–Pt/CNT catalysts. The current density of Bi–Pt/CNT (0.1:1) catalyst keeps at 41.7 mA cm^{-2} at 1800 s, which is 44.8 times higher than that of Pt/CNT catalyst (0.93 mA cm^{-2}).

The anti-poisoning ability of catalysts can be estimated by the linear current sweep method [50]. The changes in electrode potentials with time on Bi–Pt/CNT and Pt/CNT catalysts are displayed in Fig. 13. In the processes of ethanol oxidation, the accumulations of poisonous carbonaceous intermediates on the catalyst surface cause the increases in the electrode potential because the increased intermediates must be further oxidized with more OH_{ad} species to satisfy the applied currents, while the OH_{ad} species produced in the discharge of the OH^- in the solution are still not plentiful enough and the electrode potentials must rise for the formations of more OH_{ad} species [51]. Potential oscillation occurs when there exists periodically abundant adsorption of CO-like species formed during ethanol oxidation processes and the corresponding potential change to supply OH_{ad} species for the oxidation of poisonous intermediates. It is found from Fig. 13 that the potential oscillation takes place on the catalysts with no or low Bi content (Pt/CNTs,

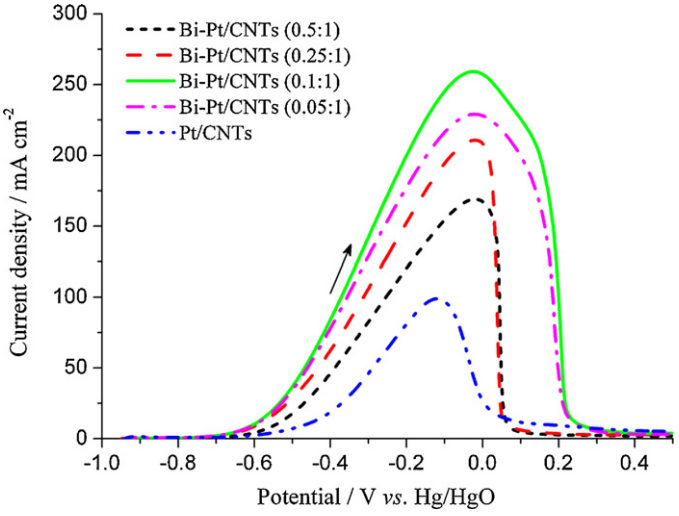

Fig. 11. Positive-going potential sweep curves of Bi–Pt/CNTs with different atomic ratios of Bi to Pt in microwave synthesis and Pt/CNTs in 1 M KOH + 1 M C_2H_5OH solution. Scan rate: 50 mV s^{-1}.

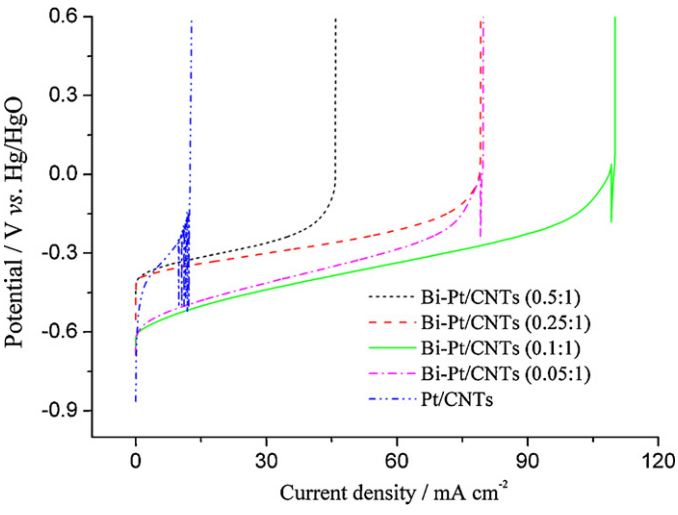

Fig. 13. Linear current sweep curves of Bi–Pt/CNTs with different atomic ratios of Bi to Pt in microwave synthesis and Pt/CNTs at the scan rate of 0.16 mA cm^{-2} s^{-1} in 1 M KOH + 1 M C_2H_5OH solution.

Bi–Pt/CNTs (0.05:1) and Bi–Pt/CNTs (0.1:1)), suggesting that Bi facilitates the adsorption of OH_{ad} species on the Pt surfaces again. For all the catalysts in Fig. 13, the current values at the turning point of the potential exhibit the trend to increase first and then decrease with the increase of Bi content. And Bi–Pt/CNT (0.1:1) catalyst shows the lowest polarization potential and the highest current density of 110 mA cm^{-2} at the point of steep hop in potential, indicating the highest catalytic activity towards ethanol oxidation and excellent tolerance towards CO-like species poisoning.

4. Conclusions

The Bi-modified Pt/CNT catalysts can be synthesized via two approaches of long-term standing and microwave treatment for as-prepared Pt/CNTs. Since Pt has a strong affinity for Bi, the irreversible adsorption of the Bi^{3+} ions occurs when they arrive at the surface of Pt/CNT aggregations. In long-term standing, the diffusion of Bi^{3+} ions is slow at room temperature so that the Bi^{3+} ions in the reactor cannot react completely. And the adsorbed Bi^{3+} ions only deposit on the outside of Pt/CNT aggregations in the form of hydroxide or oxide of Bi (III) in alkaline medium. Consequently, an adsorption saturation state is reached after standing for 5 h. In the microwave treatment, the temperature of the reactor rises rapidly to 190 °C and higher, at which the EG solution viscosity is very low and the diffusion of Bi^{3+} ions becomes very fast. The Bi^{3+} ions arriving at the surface of Pt/CNT nanoparticles can interact with Pt with strong affinity and deposit as hydroxide or oxide of Bi (III) in alkaline medium. And the Bi oxide does not deposit outside the Pt/CNT nanoparticles, instead it distributes uniformly in the entire catalysts, and the reaction can be completed in a very short time under the microwave.

The increase of Bi amount in the Bi-containing catalyst leads to the positive shift of its open circuit potential, which indicates that the Bi-containing catalyst enhance the adsorption of oxygen-containing species. These oxygen-containing species make the Bi-modified Pt/CNT catalysts have higher tolerance towards poisonous intermediates formed during EOR processes. The EOR peak of Bi–Pt/CNT (0.1:1) catalyst exhibits about 2.6 times higher specific activity (259.3 mA cm^{-2}) than the value of Pt/CNT catalyst (98.7 mA cm^{-2}). The current density on current–time curve at −0.3 V for 1800 s of Bi–Pt/CNTs (0.1:1) is even 44.8 times higher than that of Pt/CNTs.

Acknowledgement

This work was financially supported by the National Natural Science Foundation of China (No. 51072037).

Appendix A. Supplementary data

Supplementary data associated with this article can be found, in the online version, at http://dx.doi.org/10.1016/j.apcatb.2012.09.049.

References

[1] S.Q. Song, P. Tsiakaras, Applied Catalysis B: Environmental 63 (2006) 187–193.
[2] E. Antolini, Journal of Power Sources 170 (2007) 1–12.
[3] H.Q. Song, X.P. Qiu, F.S. Li, Applied Catalysis A: General 364 (2009) 1–7.
[4] S.T. Nguyen, H.M. Law, H.T. Nguyen, N. Kristian, S. Wang, S.H. Chan, X. Wang, Applied Catalysis B: Environmental 91 (2009) 507–515.
[5] Y. Wang, T.S. Nguyen, C. Wang, X. Wang, Dalton Transactions (2009) 7606–7609.
[6] S.Q. Song, W.J. Zhou, Z.H. Zhou, L.H. Jiang, G.Q. Sun, Q. Xin, V. Leontidis, S. Kontou, P. Tsiakaras, International Journal of Hydrogen Energy 30 (2005) 995–1001.
[7] J.C.M. Silva, R.F.B. De Souza, L.S. Parreira, E.T. Neto, M.L. Calegaro, M.C. Santos, Applied Catalysis B: Environmental 99 (2010) 265–271.
[8] J. Mann, N. Yao, A.B. Bocarsly, Langmuir 22 (2006) 10432–10436.
[9] L. Xin, Z. Zhang, J. Qi, D. Chadderdon, W. Li, Applied Catalysis B: Environmental 125 (2012) 85–94.
[10] S.S. Gupta, J. Datta, Journal of Power Sources 145 (2005) 124–132.
[11] Q. Tang, L. Jiang, J. Qi, Q. Jiang, S. Wang, G. Sun, Applied Catalysis B: Environmental 104 (2011) 337–345.
[12] M. Simões, S. Baranton, C. Coutanceau, Applied Catalysis B: Environmental 93 (2010) 354–362.
[13] A. Caillard, C. Coutanceau, P. Brault, J. Mathias, J.-M. Léger, Journal of Power Sources 162 (2006) 66–73.
[14] C. Coutanceau, S. Brimaud, C. Lamy, J.-M. Léger, L. Dubau, S. Rousseau, F. Vigier, Electrochimica Acta 53 (2008) 6865–6880.
[15] V. Bambagioni, C. Bianchini, A. Marchionni, J. Filippi, F. Vizza, J. Teddy, P. Serp, M. Zhiani, Journal of Power Sources 190 (2009) 241–251.
[16] R. Wlodarczyk, M. Chojak, K. Miecznikowski, A. Kolary, P.J. Kulesza, R. Marassi, Journal of Power Sources 159 (2006) 802–809.
[17] P.J. Kulesza, K. Karnicka, K. Miecznikowski, M. Chojak, A. Kolary, P.J. Barczuk, G. Tsirlina, W. Czerwinski, Electrochimica Acta 50 (2005) 5155–5162.
[18] T. Maiyalagan, International Journal of Hydrogen Energy 34 (2009) 2874–2879.
[19] D.W. Pan, J.H. Chen, W.Y. Tao, L.H. Nie, S.Z. Yao, Langmuir 22 (2006) 5872–5876.
[20] D.M. Han, Z.P. Guo, R. Zeng, C.J. Kim, Y.Z. Meng, H.K. Liu, International Journal of Hydrogen Energy 34 (2009) 2426–2434.
[21] M.C. Figueiredo, J. Souza-Garcia, V. Climent, J.M. Feliu, Electrochemistry Communications 11 (2009) 1760–1763.
[22] X.W. Yu, P.G. Pickup, Electrochimica Acta 55 (2010) 7354–7361.
[23] Y.L. Du, B.Q. Su, N. Zhang, C.M. Wang, Applied Surface Science 255 (2008) 2641–2645.
[24] B. Peng, J.Y. Wang, H.X. Zhang, Y.H. Lin, W.B. Cai, Electrochemistry Communications 11 (2009) 831–833.
[25] I. Kerbach, V. Climent, J.M. Feliu, Electrochimica Acta 56 (2011) 4451–4456.
[26] L. Demarconnay, S. Brimaud, C. Coutanceau, J.-M. Léger, Journal of Electroanalytical Chemistry 601 (2007) 169–180.
[27] M.M. Tusi, N.S.O. Polanco, S.G. da Silva, E.V. Spinacé, A.O. Neto, Electrochemistry Communications 13 (2011) 143–146.
[28] Y.L. Du, C.M. Wang, Materials Chemistry and Physics 113 (2009) 927–932.
[29] A. López-Cudero, F.J. Vidal-Iglesias, J. Solla-Gullón, E. Herrero, A. Aldaz, J.M. Feliu, Physical Chemistry Chemical Physics 11 (2009) 416–424.
[30] M. Simões, S. Baranton, C. Coutanceau, Applied Catalysis B: Environmental 110 (2011) 40–49.
[31] D.L. Martins, H.M. Alvarez, L.C.S. Aguiar, O.A.C. Antunes, Applied Catalysis A: General 408 (2011) 47–53.
[32] D.M. Gu, Y.Y. Chu, Z.B. Wang, Z.Z. Jiang, G.P. Yin, Y. Liu, Applied Catalysis B: Environmental 102 (2011) 9–18.
[33] E. Lebègue, S. Baranton, C. Coutanceau, Journal of Power Sources 196 (2011) 920–927.
[34] S. Harish, S. Baranton, C. Coutanceau, J. Joseph, Journal of Power Sources 214 (2012) 33–39.
[35] R.N. Singh, A. Singh, Anindita, International Journal of Hydrogen Energy 34 (2009) 2052–2057.
[36] V. Datsyuk, M. Kalyva, K. Papagelis, J. Parthenios, D. Tasis, A. Siokou, I. Kallitsis, C. Galiotis, Carbon 46 (2008) 833–840.
[37] C.W. Yang, D.L. Wang, X.G. Hu, C.S. Dai, L. Zhang, Journal of Alloys and Compounds 448 (2008) 109–115.
[38] C.T. Hsieh, W.M. Hung, W.Y. Chen, International Journal of Hydrogen Energy 35 (2010) 8425–8432.
[39] Y. Verde, G. Alonso, V. Ramos, H. Zhang, A.J. Jacobson, A. Keer, Applied Catalysis A: General 277 (2004) 201–207.
[40] J.T. Richardson, M. Garrait, J.-K. Hung, Applied Catalysis A: General 255 (2003) 69–82.
[41] L. Demarconnay, C. Coutanceau, J.-M. Léger, Electrochimica Acta 53 (2008) 3232–3241.
[42] M. Chatterjee, A. Chatterjee, S. Ghosh, I. Basumallick, Electrochimica Acta 54 (2009) 7299–7304.
[43] F. Vigier, C. Coutanceau, F. Hahn, E.M. Belgsir, C. Lamy, Journal of Electroanalytical Chemistry 563 (2004) 81–89.
[44] A. Dutta, S.S. Mahapatra, J. Datta, International Journal of Hydrogen Energy 36 (2011) 14898–14906.
[45] S. Cherevko, X.L. Xing, C.H. Chung, Electrochimica Acta 56 (2011) 5771–5775.
[46] Z.Y. Zhang, L. Xin, K. Sun, W.Z. Li, International Journal of Hydrogen Energy 36 (2011) 12686–12697.
[47] L. Jiang, A. Hsu, D. Chu, R. Chen, International Journal of Hydrogen Energy 35 (2010) 365–372.
[48] Z.G. Chen, X.P. Qiu, B. Lu, S.C. Zhang, W.T. Zhu, L.Q. Chen, Electrochemistry Communications 7 (2005) 593–596.
[49] T.J. Schmidt, R.J. Behm, B.N. Grgur, N.M. Markovic, P.N. Ross Jr., Langmuir 16 (2000) 8159–8166.
[50] M. Krausa, W. Vielstich, Journal of Electroanalytical Chemistry 399 (1995) 7–12.
[51] Y.Y. Huang, J.D. Cai, Y.L. Guo, International Journal of Hydrogen Energy 37 (2012) 1263–1271.